JACS
JOURNAL OF THE AMERICAN CHEMICAL SOCIETY
Article
pubs.acs.org/JACS

Development of Specific, Irreversible Inhibitors for a Receptor Tyrosine Kinase EphB3

Alvin Kung,[†] Ying-Chu Chen,[†] Marianne Schimpl,[‡] Feng Ni,[†] Jianfa Zhu,[†] Maurice Turner,[†] Henrik Molina,[⊥] Ross Overman,[§] and Chao Zhang*[,†,∥]

[†]Department of Chemistry and Loker Hydrocarbon Research Institute, and [∥]Department of Biological Sciences, University of Southern California, Los Angeles, California 90089, United States

[‡]Discovery Sciences, Innovative Medicines and Early Development Biotech Unit, AstraZeneca, Building 310, Cambridge Science Park, Milton Road, Cambridge CB4 0WG, United Kingdom

[§]Discovery Sciences, Innovative Medicines and Early Development Biotech Unit, AstraZeneca, Alderley Park, Macclesfield, Cheshire SK10 4TG, United Kingdom

[⊥]Proteomic Resource Center, The Rockefeller University, New York, New York 10065, United States

Supporting Information

ABSTRACT: Erythropoietin-producing human hepatocellular carcinoma (Eph) receptor tyrosine kinases (RTKs) regulate a variety of dynamic cellular events, including cell protrusion, migration, proliferation, and cell-fate determination. Small-molecule inhibitors of Eph kinases are valuable tools for dissecting the physiological and pathological roles of Eph. However, there is a lack of small-molecule inhibitors that are selective for individual Eph isoforms due to the high homology within the family. Herein, we report the development of the first potent and specific inhibitors of a single Eph isoform, EphB3. Through structural bioinformatic analysis, we identified a cysteine in the hinge region of the EphB3 kinase domain, a feature that is not shared with any other human kinases. We synthesized and characterized a series of electrophilic quinazolines to target this unique, reactive feature in EphB3. Some of the electrophilic quinazolines selectively and potently inhibited EphB3 both in vitro and in cells. Cocrystal structures of EphB3 in complex with two quinazolines confirmed the covalent linkage between the protein and the inhibitors. A "clickable" version of an optimized inhibitor was created and employed to verify specific target engagement in the whole proteome and to probe the extent and kinetics of target engagement of existing EphB3 inhibitors. Furthermore, we demonstrate that the autophosphorylation of EphB3 within the juxtamembrane region occurs in *trans* using a specific inhibitor. These exquisitely specific inhibitors will facilitate the dissection of EphB3's role in various biological processes and disease contribution.

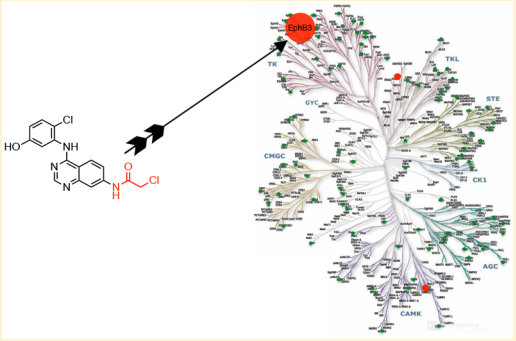

INTRODUCTION

Erythropoietin-producing human hepatocellular (Eph) receptors and their ligands ephrins orchestrate various dynamic cellular events, including cell protrusion, migration, proliferation, and cell-fate determination.[1,2] There is a strong association between dysregulation of Eph receptors and cell proliferation, anti-apoptotic repercussions, and ultimately oncogenic transformation.[3−8] For example, EphA4 and EphB4 have been found to contribute to proliferation or metastasis of multiple forms of cancer.[6] However, for another family member, EphB3, recent studies have documented conflicting roles in cancerogenesis.[9−12] While earlier studies suggested that overexpression of EphB3 in non-small-cell lung cancer promoted metastasis by enhancing the tumor's survival and migratory capabilities,[10] a recent report implicates EphB3 as a tumor suppressor.[11] The exact role of EphB3 in cancer remains controversial at the moment.

Binding of ephrin to Eph is thought to promote receptor oligomerization, resulting in autophosphorylation at multiple sites in the cytoplasmic domains, including the juxtamembrane region, the kinase domain, and the SAM domain.[13] In principle, RTK autophosphorylation can operate in *cis* within one receptor or in *trans* between two neighboring receptors. Studies with prototypical RTKs such as the epidermal growth factor receptor (EGFR) and the insulin receptor elucidated that the autophosphorylation mechanism varies depending on the position of the phosphosites.[14−16] However, the activation mechanism for Eph receptors has not been fully investigated to our knowledge.

The Eph receptors have been studied using various genetic methods, including protein overexpression, gene knockout, and knockdown.[1,5] These studies provided valuable information on

Received: May 27, 2016
Published: August 1, 2016

ACS Publications © 2016 American Chemical Society

DOI: 10.1021/jacs.6b05483
J. Am. Chem. Soc. 2016, 138, 10554−10560

the cellular functions and disease relevance of Ephs. However, the dramatic change in protein levels and slow genetic perturbation can cause either overexpression phenotype or cellular compensations, which confounds interpretation of the experimental results.[17] Use of pharmacological modulators of Eph can minimize these complications as they take effect rapidly without affecting protein levels.[18] Although multiple inhibitors of Eph kinases have been reported in the literature, they invariably suffer from a lack of specificity for individual Eph isoforms due to the high conservation within Eph kinase domains.[7,19] The lack of isoform-selective inhibitors has prevented pharmacological mapping of functions of individual Eph kinases.

A chemical–genetic approach that generates potent and specific inhibitors of protein kinases by targeting nonconserved cysteine residues has been previously described.[17,20,21] The approach has been employed to generate potent irreversible inhibitors of a number of protein kinases including Rsk, Nek2, c-Src, a drug-resistant mutant (T790M) of EGFR, JNK, and Cdk7.[22−27] Our kinome-wide sequence analysis revealed additional cysteine-containing kinases that would be amenable to this approach. In particular, we noticed that EphB3 contains a cysteine residue near the end of the hinge region, a feature that is shared by only two other kinases, LKB1 and PINK1, in the entire human kinome (Figure 1A and data not shown).

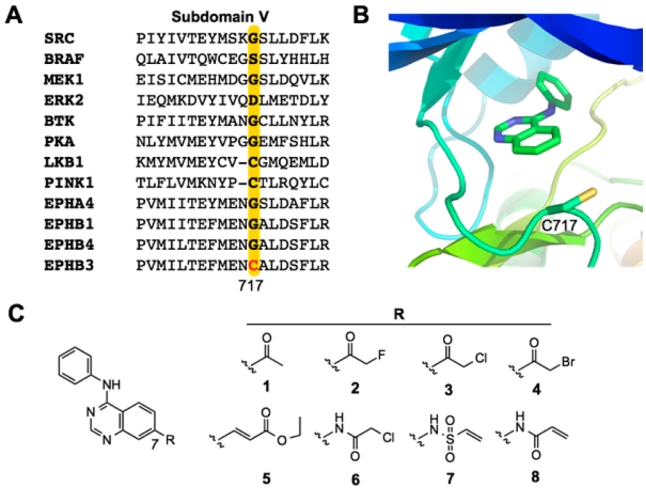

Figure 1. Design of specific, electrophilic inhibitors of EphB3 guided by structural bioinformatics. (A) Partial sequence alignment of EphB3 with 10 other protein kinases within the subdomain V. The position where EphB3 contains a cysteine (C717) is highlighted. (B) Binding model of 4-anilinoquinazoline to the active site of EphB3 with C717 highlighted. (C) Quinazolines containing various electrophiles at position 7 designed to covalently target C717 in EphB3.

Importantly, the cysteine residue in LKB1 and PINK1 is expected to point away from the active site and to not be as accessible as that of EphB3 because of a deletion in the hinge region of these two serine/threonine kinases compared to tyrosine kinases (Figure 1A). Thus, EphB3 contains a unique reactive feature that can be exploited for the development of specific irreversible inhibitors of EphB3. Herein, we report the design, synthesis, optimization, and biological characterization of a series of electrophilic quinazolines as irreversible inhibitors of EphB3. Our optimized inhibitors exhibit exquisite specificity at inhibiting EphB3 not only within the human kinome but also in the whole proteome. These specific inhibitors were employed to measure the engagement of various kinase inhibitors to EphB3 and probe the activation mechanism of EphB3 in cells.

RESULTS AND DISCUSSION

Synthesis of Electrophilic EphB3 Inhibitors. To identify an appropriate scaffold for covalently targeting the unique cysteine C717 in EphB3, a dozen inhibitors with different pharmacophores, such as pyrazolopyrimidine, bisanilinopyrimidine, and quinazoline, were docked into the EphB3 active site based on a crystal structure that has been recently reported.[28] A combination of automated docking using AutoDock Vina and manual docking in Pymol was employed to generate and analyze binding poses of the inhibitor scaffolds. The docking score (or potential steric clash), distance from the C717 thiol group, and ease of derivatization were weighed to evaluate the various scaffolds. The quinazoline, which constitutes the core of the anticancer drug gefitinib, erlotinib and lapatinib,[29] was selected for its good fit into the EphB3 active site and the proximity of its 7 position to the unique cysteine residue based on the docking mode (Figure 1B). A panel of quinazolines that contain various electrophilic groups at the C7 position were thus designed to irreversibly target C717 in EphB3 (Figure 1C). These electrophiles include halomethylketones, acrylate, chloroacetamide, vinylsulfonamide, and acrylamide that exhibit varying distance from the quinazoline core to the electrophilic carbons and distinct stereochemical requirements for reaction with the cysteine thiol group. The quinazolines were chemically synthesized using two different routes (Schemes S1 and S2).

Selective Inhibition of EphB3 in Vitro. Having synthesized the panel of electrophilic quinazolines, we first characterized their inhibition of the EphB3 kinase in vitro. Recombinant EphB3 kinase was expressed and purified from *Escherichia coli*, as previously described.[28] The electrophilic quinazolines were screened for inhibition against the EphB3 kinase using an in vitro kinase assay based on the phosphorylation of a peptide substrate with [γ-^{32}P] ATP.[30] The quinazolines caused different levels of inhibition against the EphB3 kinase (Figure 2A). Three quinazolines that contain halomethylketone (**2** and **3**) or chloroacetamide (**6**) inhibited EphB3 kinase activity by more than 80% when used at 2 μM, while the other quinazolines in the panel caused little or moderate inhibition against EphB3 under the same conditions (Figure 2A). The varying degrees of EphB3 inhibition by these quinazolines is consistent with the notion that only certain electrophiles are poised to form covalent interaction with C717. We next determined the IC_{50} values of the three most potent quinazolines along with the non-electrophilic methylketone **1** against EphB3 (Table 1). The halomethylketones **2** and **3** inhibited EphB3 with apparent IC_{50} values of 415 and 6 nM, respectively. The potency difference is consistent with the reactivity difference between these two halomethylketone groups as chlorine is a much better leaving group than fluorine for the nucleophilic substitution reaction. The chloroacetamide-containing **6** had an intermediate potency at inhibiting EphB3 (IC_{50} = 55 nM) compared to the two halomethylketones. In contrast, the non-electrophilic quinazoline **1** that differs from **2** and **3** by a single atom substitution inhibited EphB3 poorly (IC_{50} > 10 μM).

To determine the importance of the cysteine (C717) for inhibition of EphB3, we measured the electrophilic quinazolines' inhibition against a mutant form of EphB3 in which this cysteine was mutated to serine. After being expressed and

DOI: 10.1021/jacs.6b05483
J. Am. Chem. Soc. 2016, 138, 10554−10560

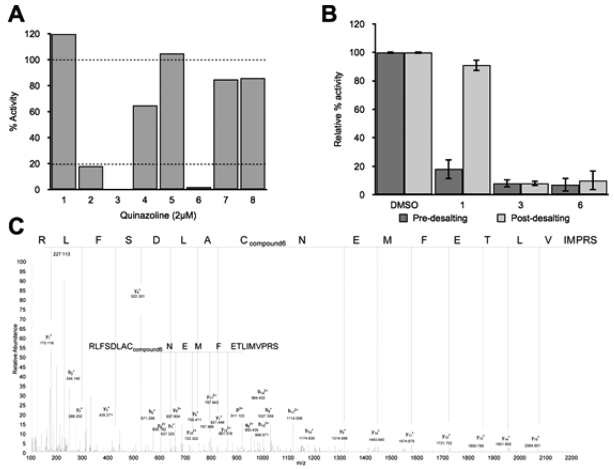

Figure 2. Electrophilic quinazolines caused covalent and irreversible inhibition of EphB3 in vitro. (A) Screening of the quinazolines (at 2 μM) for inhibition against the EphB3 kinase. Kinase activity was normalized to the DMSO control. (B) Inhibition of EphB3 by **3** (10 μM) and **6** (10 μM) could not be reversed by washout as with **1** (100 μM). Activity was normalized to the DMSO control (mean ± SD from triplicates). (C) Tandem mass spectrum of the **6**-modified C717-containing triply charged tryptic peptide SRPV-MILTEFMENC$_{compound6}$ALDSFLR measured at m/z 916.77374 (mass accuracy: 1.0 ppm). Fragment ions (y and b) are annotated in the spectrum.

Table 1. IC_{50} (nM) Values of Quinazolines against Various Forms of Eph Kinases in Vitro[a]

compound	EphB3 WT	EphB3 C717S	EphB4 WT	EphA4 WT
1	>10000	>10000	>10000	>10000
2	415	>10000	>10000	>10000
3	6	>10000	>10000	>10000
6	55	>10000	>10000	>10000

[a]Disk assay based on phosphorylation of a peptide substrate with [γ-^{32}P] ATP was used. IC_{50} values were calculated using GraphPad Prism.

purified from *Escherichia coli*, EphB3 C717S was found to have activity comparable to that of the wild-type and was not significantly inhibited by any quinazolines in the panel at 10 μM (Figure S1).[28] Finally, none of the electrophilic quinazolines potently inhibit EphA4 and EphB4, two other Eph kinases that are missing a cysteine at the homologous position (Table 1). Together, these results suggest that C717 is essential for potent inhibition of EphB3 by the electrophilic quinazolines **2**, **3**, and **6**.

Covalent Inhibition of EphB3 by the Quinazolines. We examined the reversibility of EphB3 inhibition by the electrophilic quinazolines by conducting washout experiments. Upon washout, **1** lost its inhibition against EphB3, consistent with it being a reversible inhibitor (Figure 2B). In contrast, **3** and **6** retained potent inhibition of EphB3 after washing out the inhibitors, indicating covalent inhibition. Furthermore, 1 h preincubation with EphB3 kinase decreased the apparent IC_{50} value of **2** by 5-fold, showing that the inhibition is time-dependent, as expected for a covalent inhibitor (Figure S2). To verify the mode of covalent inhibition, we used mass spectrometry to measure the modification of EphB3 by the electrophilic quinazolines. The EphB3 protein was incubated with **3** or **6** and then subjected to ESI-MS analysis to determine the whole protein mass. We observed mass increases of 259 and 275 Da of the EphB3 kinase upon treatment with **3** and **6**, respectively (Figure S3). These mass shifts are consistent with covalent modification of EphB3 by these two electrophilic quinazolines. Furthermore, incubation of the EphB3 protein with **6** followed by trypsinization and LC-MS/MS analysis revealed selective covalent modification of the C717-containing tryptic peptide (Figure 2C and Figure S3). Together, these results provide definitive proof that the electrophilic quinazolines irreversibly inhibit EphB3 by covalently modifying C717.

Potent Inhibition of EphB3 in Cells. Having established the potent and selective inhibition of the EphB3 kinase by the electrophilic quinazolines in vitro, we went on to investigate the inhibition of the full-length receptor by these compounds in cells. After transfecting EphB3 into HEK293 cells, we verified that the resulting cells expressed EphB3 and responded to the treatment with ephrin-B2 by inducing autophosphorylation of the receptor (Figure 3A). Screening the quinazolines at a

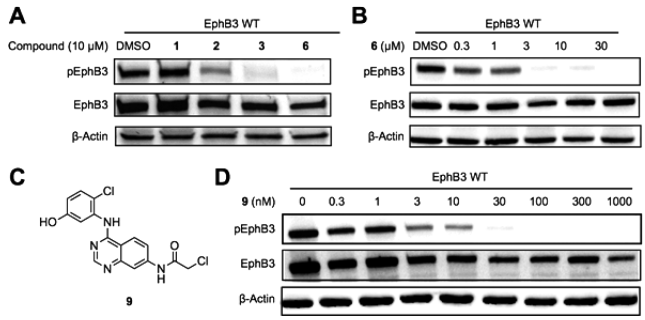

Figure 3. Modification of **6** led to the identification of **9**, a much more potent inhibitor of EphB3 in cells. (A) Activity of EphB3 WT is inhibited by the electrophilic quinazolines (**2**, **3**, and **6**) but not by the non-electrophilic analogue **1** in cells. (B) Compound **6** inhibited the autophosphorylation of EphB3 WT in a dose-dependent manner with an EC_{50} of 170 nM. (C) Chemical structure of **9**, a derivative of **6**. (D) **9** exhibited potent inhibition of EphB3 activity with an EC_{50} of 3 nM in cells. Cell lysate was resolved by SDS-PAGE, transferred to a nitrocellulose membrane, and immunoblotted with antibodies for phospho-Eph (pEphB3), EphB3, and β-actin.

concentration of 10 μM revealed that **2**, **3**, and **6** inhibited EphB3 autophosphorylation to different degrees (Figure 3A). Specifically, **3** and **6** abolished the EphB3 phosphorylation, while **2** caused partial blockade. The SAR of the quinazoline series at inhibiting EphB3 activity in cells is consistent with that from the in vitro studies. Furthermore, **3** and **6** inhibited the autophosphorylation of EphB3 in a dose-dependent manner with apparent EC_{50} values of 300 and 170 nM, respectively (Figure S4 and Figure 3B). This coincides with the non-electrophilic control compound **1** incapable of inhibiting EphB3 (Figure S5). These results suggest that the electrophilic quinazolines can readily cross plasma membrane and reach the cytoplasmic kinase domain of EphB3 in live cells.

Importantly, **3** and **6** do not significantly affect autophosphorylation of the C717S mutant of full-length EphB3 receptor at concentrations up to 10 μM, supporting the notion that potent inhibition of EphB3 by electrophilic quinazolines depends on C717 not only in vitro but also in cells (Figure S6). Moreover, none of the studied quinazolines inhibited autophosphorylation of EphB1, a close homologue of EphB3 that does not contain a cysteine at the position corresponding to C717 of EphB3, in cells at 10 μM (Figure S7). Taken

DOI: 10.1021/jacs.6b05483
J. Am. Chem. Soc. 2016, 138, 10554−10560

together, these results suggest that **3** and **6** are potent and selective inhibitors of EphB3 in cells.

We next sought to improve the potency of EphB3 inhibition by modifying the inhibitor structure, particularly the anilino group at the 4 position. On the basis of reported SAR for a series of EphB4 inhibitors and docking analysis,[31] we synthesized a few analogues of **6** (Scheme S2). Among these, one derivative **9** that contains chloro and hydroxyl substituents on the phenyl ring improved potency dramatically (Figure 3C,D). A dose−response study indicated that **9** had an EC_{50} value of 3 nM at inhibiting EphB3 autophosphorylation in cells. Thus, the subtle modifications to the aniline group dramatically improved the potency of 7-chloroacetamido quinazoline's inhibition against EphB3.

Crystal Structures of EphB3 Bound to Inhibitors. To elucidate the binding interactions between our inhibitors and EphB3 kinase, we solved the cocrystal structures of the EphB3 kinase domain with **3** and **6**. After being expressed and purified to homogeneity as previously described,[28] the EphB3 kinase was incubated with a 3-fold molar excess of **3** and **6** before crystallization. EphB3−**3** and EphB3−**6** crystals diffracted to resolution of 1.9 and 2.3 Å, respectively, and belonged to space group $P2_12_12_1$ (Table S2). The structures were solved by molecular replacement using the apo structure of EphB3 as the model.[28] The protein conformations are similar to the apo structure (rmsd values for the α carbon of 260 amino acids of EphB3−**3** and EphB3−**6** compared to apo kinase are 0.63 and 0.50 Å, respectively). As observed for the apo structure, EphB3 is in the inactive DFG-out conformation. The cocrystal structures revealed strong electron density between C717 and the electrophilic carbon in **3** and **6** and thus unambiguously verified the formation of covalent bonds (Figure 4A,B).

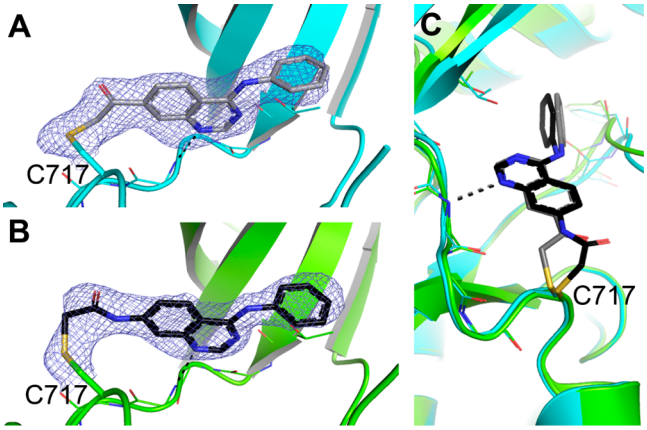

Figure 4. Crystal structures of EphB3 in complex with electrophilic quinazolines verify the formation of a covalent bond to C717. (A) Crystal structure of the EphB3−**3** complex. (B) Crystal structure of the EphB3−**6** complex. (C) Overlay of the two structures. $|2F_0-F_c|$ electron density is shown as blue mesh (contoured at 1 σ) in (A,B). The protein is shown in cartoon representation, while the ligand and key residues in the hinge region and the DFG motif are shown as sticks.

Interestingly, despite the different sizes of the electrophiles in the two inhibitors, their quinazoline cores are virtually superimposable to each other (Figure 4C), supporting the notion that the binding of the quinazoline to the EphB3 active site is crucial for directing the electrophile for reaction with the thiol group of C717.

Kinome Inhibition Profiling. To determine the inhibitors' selectivity profiles, we tested **6** and **9** for inhibition against a panel of 98 diverse human kinases that cover all major branches of the kinome phylogenetic tree using the SelectScreen Kinase Profiling Services from ThermoFisher. The results indicate that **6** at 300 nM only significantly inhibited two kinases, EphB3 and EGFR, out of the 98 (Figure 5A). However, inhibition of EGFR

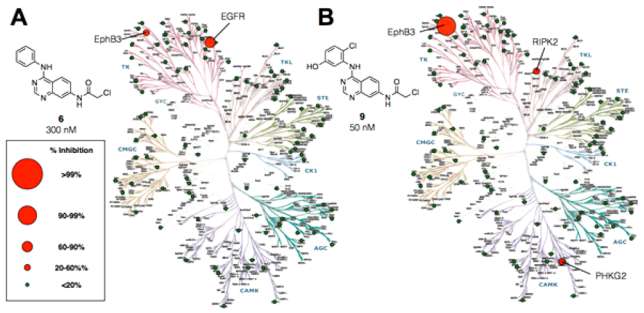

Figure 5. Graphical representations of the kinase inhibition profiles for **6** and **9**. (A) Two major targets of **6** at 300 nM are EphB3 and EGFR, with the latter being inhibited more. (B) **9** at 50 nM causes foremost inhibition of EphB3 among the tested kinases. Only two other kinases, RIPK2 and PHKG2, are significantly inhibited by **9** but to a much lesser extent. Percentage inhibition of a diverse panel of 98 kinases is mapped to the human kinome tree to visualize inhibitor selectivity. The larger the circles are, the stronger the inhibition. Kinase dendrogram was adapted and reproduced with permission from Cell Signaling Technology Inc. (http://www.cellsignal.com).

by **6** appears to be stronger than that of EphB3, the target of our interest. This off-target inhibition is probably due to the extremely high affinity of quinazoline for EGFR, reflected by the fact that the majority of clinically used small-molecule inhibitors of EGFR contain a quinazoline core.[29] In contrast, the optimized inhibitor **9** exhibited more specific and potent inhibition of EphB3 (Figure 5B). At 50 nM, **9** caused 98% inhibition of EphB3 with only two other kinases (RIPK2 and PHKG2) being inhibited by over 20% in the panel. Sequence and structure analyses revealed an absence of cysteine residues near the end of the hinge region in RIPK2 and PHKG2, suggesting that their binding to **9** is driven by noncovalent interactions. These results indicate that our chemical optimization led to not only improved potency but also exquisite specificity at inhibiting EphB3 within the human kinome.

PINK1 and LBK1, the two kinases that appear to contain a cysteine at the position homologous to C717 in EphB3, are not predicted to be inhibited by the electrophilic quinazolines because of a deletion in their hinge region from EphB3 (Figure 1A). These two kinases were not among the profiled panel of kinases, however. We thus measured the inhibition of LBK1 by **6** and **9** in vitro. Dose−response studies indicate that **6** and **9** both have IC_{50} values greater than 10 μM against LKB1, thus confirming that our inhibitors do not potently inhibit kinases that contain a shorter hinge region despite the presence of a homologous cysteine (Figure S8).

Clickable Probe To Monitor Target Engagement. When used at high concentrations, electrophilic compounds may nonspecifically label cellular proteins, especially the abundant ones.[32,33] To confirm target engagement and determine proteomic selectivity of our inhibitors, we chose to derivatize **9** with a terminal alkyne group, which is amenable to

DOI: 10.1021/jacs.6b05483
J. Am. Chem. Soc. 2016, 138, 10554−10560

the copper-catalyzed azide−alkyne cycloaddition (CuAAC) click reaction. Based on the cocrystal structure (Figure 4), we opted to attach the alkyne tag at the 6 position of the quinazoline that is solvent-exposed and predicted to be accessible for the click reaction. The resulting quinazoline probe **10** was synthesized in seven steps (Scheme S3). **10** still caused potent inhibition (IC_{50} ~ 10 nM) of EphB3 activity in cells, suggesting that the alkyne attachment caused only a slight decrease in potency (Figure 6A). We first employed **10** to

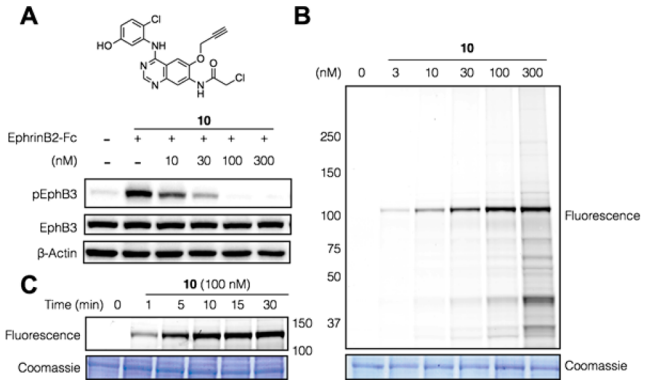

Figure 6. Inhibition and specific labeling of EphB3 by the clickable probe **10** in cells. (A) **10**, whose structure is shown at the top, inhibited the autophosphorylation of EphB3 WT in a dose-dependent manner with an IC_{50} of 10 nM (calculated with GraphPad Prism). (B) Dose-dependent labeling of EphB3 in HEK293 cells as revealed by in-gel fluorescence imaging. (C) Time-dependent labeling with **10** at 100 nM of EphB3 in HEK293 cells as revealed by in-gel fluorescence imaging. Coomassie blue staining shows equal protein loading in (B,C).

monitor its engagement of the target protein EphB3 in cells. After the treatment of EphB3-expressing cells with **10** at various concentrations, the cells were lysed, clicked with TAMRA-azide, resolved by SDS-PAGE, and scanned for a fluorescence image.[33] We observed only one major fluorescent band of ~110 kDa in the gel when cells were treated with up to 100 nM of **10** (Figure 6B). The fact that this band is absent in the parental HEK293 cells that do not express EphB3 strongly suggests that the probe-labeled protein is EphB3 (Figure S9). The sensitivity of this small-molecule probe is highlighted by the fact that **10** detected low levels of endogenous EphB3 proteins in two cell lines while an EphB3 antibody failed to do so (Figure S10). The low levels of EphB3 protein that we detected in the adult cell lines are consistent with the expression pattern of EphB3 that is believed to peak during the embryonic development, particularly in the brain.[34,35] Higher concentrations (>100 nM) of the probe caused nonspecific labeling of other cellular proteins as expected for electrophilic compounds (Figure 6B). Time-course experiment demonstrated that **10** could engage EphB3 in cells within 5 min (Figure 6C). Together, these results suggest that **10** is a probe that can engage EphB3 potently, specifically, and rapidly in cells.

We next used **10** as a probe to measure the occupancy of EphB3 by various inhibitors in live cells. Treating EphB3-expressing HEK293 cells with various concentrations of an irreversible inhibitor **9** led to the occupancy of a fraction of the target kinase. Subsequent addition of 100 nM of **10** would completely label the remaining fraction of EphB3. After click reaction and gel electrophoresis, the fluorescence intensity of the target band was normalized to the mock treatment to read out the fraction of EphB3 that was not occupied by **9**. From the dose−response study, we were able to determine the concentration at which 50% of the target is occupied in cells (Figure 7A). This value of 6 nM is similar to the IC_{50} value (3

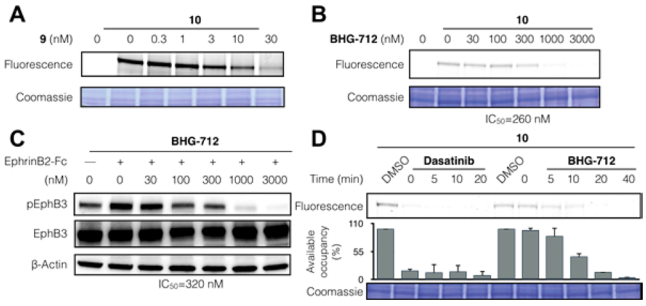

Figure 7. Competition experiments reveal the extent and kinetics of EphB3 engagement by different types of inhibitors in HEK293 cells. (A) Dose-dependent occupancy of EphB3 by **9** in cells as revealed by pulse-chase experiments and in-gel fluorescence imaging. **10** was used at 100 nM. (B) Increasing concentrations of BHG-712 could compete off EphB3 labeling by **10** (10 nM) in cells with an IC_{50} of 260 nM (calculated with GraphPad Prism). (C) BHG-712 blocked EphB3 autophosphorylation in a dose-dependent manner in cells with an IC_{50} of 320 nM (calculated with GraphPad Prism). Cell lysate was resolved by SDS-PAGE, transferred to nitrocellulose membrane, and immunoblotted with antibodies for pEphB3, EphB3, and β-actin. (D) Competition experiments revealed different kinetics of target engagement by two kinase inhibitors, dasatinib and BHG-712, in cells. Ten nanomolar of **10** was used. Fluorescence image from one representative experiment is shown. Fluorescence intensity was quantified for the three repeats, averaged, and normalized to the DMSO treatment. Coomassie blue staining shows equal protein loading in (A,B,D).

nM) measured for **9** at inhibiting EphB3 autophosphorylation in cells. Probe **10** was also used to measure the occupancy of EphB3 by a reversible inhibitor BHG-712 in cells. Since BHG-712 and **10** compete for binding to the same site in EphB3, increasing concentrations of BHG-712 should diminish EphB3 labeling by **10** with the extent of inhibition reflecting target occupancy by BHG-712. Indeed, we observed dose-dependent inhibition of probe labeling of EphB3 by BHG-712. The IC_{50} value determined for probe labeling is 260 nM, which agrees well with the IC_{50} value of BHG-712 at inhibiting EphB3 autophosphorylation (Figure 7B,C). Together, these results imply that that extent of EphB3 occupancy by an inhibitor correlates well with the extent of inhibition of its autophosphorylation, consistent with a previous study using EGFR inhibitors.[24]

We further used **10** to measure the target engagement kinetics of two types of kinase inhibitors. Type I kinase inhibitors are known to bind exclusively to the ATP pocket, whereas type II inhibitors additionally bind to an allosteric pocket.[36] Binding of type I inhibitors to kinases is often rapid because the ATP pocket tends to be readily accessible in the native state of the kinase. In contrast, type II inhibitors are often associated with slow binding kinetics since the allosteric pocket becomes accessible only upon a conformational change involving an outward movement of the conserved DFG motif.[37] Pretreatment of EphB3-expressing cells with 30 nM of a type I inhibitor dasatinib for various lengths of time followed by addition of **10** showed that inhibition of EphB3 labeling was insensitive to preincubation duration, indicating instantaneous

DOI: 10.1021/jacs.6b05483
J. Am. Chem. Soc. 2016, 138, 10554−10560

target engagement by dasatinib in cells (Figure 7D). Analogous experiments with BHG-712 indicated that a preincubation of over 10 min was required to effectively block EphB3 labeling by **10**. A similar preincubation is also required for BHG-712 to effectively compete off the labeling of EphB3 by **10** in cell lysate (Figure S11). These results suggest that it takes more than 10 min for BHG-712 to engage the target of EphB3 in both cell lysate and live cells, consistent with the prediction that BHG-712 is a type II kinase inhibitor based on its structural features. Furthermore, they highlight that our probe can be used to monitor the target engagement kinetics of different types of kinase inhibitors in cells, which is difficult to achieve with other methods.

Elucidation of EphB3 Autophosphorylation Mechanism. We set out to investigate the activation mechanism of EphB3 using our specific inhibitors. We first demonstrated that fusion of a stable cytochrome b_{562}RIL (BRIL) domain to EphB3 did not significantly affect the ability of the receptor to autophosphoryate (Figure S12).[38] Furthermore, a phospho-specific antibody that recognizes EphB3 phosphorylated at Y608 and Y614 in the juxtamembrane segment revealed that 100 nM of **9** abolished the autophosphorylation at those two sites of wild-type EphB3 but had little effects on the C717S mutant. When two copies of wild-type EphB3 (BRIL-tagged or not) were coexpressed in HEK293 cells, the autophosphorylation of both receptors at Y608 and Y614 was abolished by 100 nM of **9** (Figure 8). As expected, the autophosphorylation

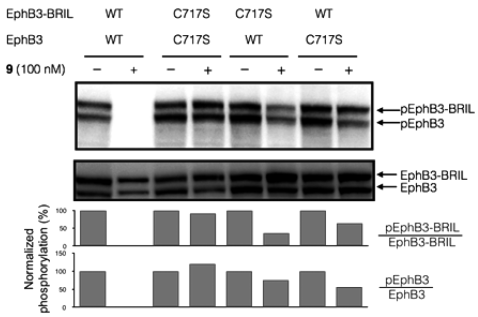

Figure 8. Use of a specific inhibitor **9** to elucidate the mechanism underlying EphB3 autophosphorylation. HEK293 cells transfected with two EphB3 variants were treated with 100 nM of **9** for 1 h before lysis. Cell lysate was resolved by SDS-PAGE, transferred to nitrocellulose membrane, and blotted with antibodies for pEphB3 and total EphB3. Relative phosphorylation levels are shown underneath the Western blots. Band intensities for phospho- and total EphB3 were quantified with their ratios normalized to that of the control (DMSO treatment).

of two C717S mutants was not affected at all by 100 nM of **9**. With cells expressing one WT and one C717S form of EphB3 (BRIL-fused or nonfused), addition of 100 nM **9** caused partial inhibition of both receptors (Figure 8). Our results are consistent with the *trans* autophosphorylation model because the *cis* model predicts a selective blockade of autophosphorylation of the WT receptor.

CONCLUSION

In summary, by covalently targeting a unique reactive feature in a receptor tyrosine kinase EphB3, we were able to identify inhibitors that exhibited high selectivity toward EphB3 not only among protein kinases but also in the entire proteome. Our rigorous and thorough characterizations verified the exquisite specificity of these inhibitors, assuring their application in biological studies. We solved the crystal structures of EphB3 in complex with covalent inhibitors for the first time. In addition to verifying the covalent linkage, these covalent complex structures can guide the design of analogous electrophilic inhibitors for targeting cysteine in proteins. Beyond generating and characterizing these covalent EphB3 inhibitors, we employed them to probe drug−target engagement and investigate the mechanism of receptor activation in an innovative way. Using a clickable probe, we were able to measure the extent and kinetics of EphB3 engagement by different types of kinase inhibitors in cells. One specific inhibitor of EphB3 allowed us to reveal that the autophosphorylation of the receptor in the juxtamembrane segment occurred in *trans*. These exquisitely specific inhibitors will accelerate pharmacological characterization of the roles of EphB3 in various biological processes such as neural development and tumorigenesis.

ASSOCIATED CONTENT

Supporting Information

The Supporting Information is available free of charge on the ACS Publications website at DOI: 10.1021/jacs.6b05483.

Experimental methods, additional figures, and analyses (PDF)

AUTHOR INFORMATION

Corresponding Author

*zhang.chao@usc.edu

Notes

The authors declare no competing financial interest.

ACKNOWLEDGMENTS

We thank Prof. B. Wang (Case Western University) and F. Sicheri (University of Toronto) for providing the constructs of EphB3 and EphA4, respectively. We thank Prof. G. Parkash (University of Southern California) for providing ephrin-B2, and M. Greenberg (Harvard University) for anti-phosphoEphB3. We thank Prof. K.M. Shokat and Ms. B. Levin (University of California, San Francisco) for help with mass spectrometry data collection. This work was supported in part by National Science Foundation (CHE-1455306), American Cancer Society (IRG-58-007-51), and University of Southern California.

REFERENCES

(1) Pasquale, E. B. *Nat. Rev. Mol. Cell Biol.* **2005**, *6*, 462.
(2) Kullander, K.; Klein, R. *Nat. Rev. Mol. Cell Biol.* **2002**, *3*, 475.
(3) Coulthard, M. G.; Morgan, M.; Woodruff, T. M.; Arumugam, T. V.; Taylor, S. M.; Carpenter, T. C.; Lackmann, M.; Boyd, A. W. *Am. J. Pathol.* **2012**, *181*, 1493.
(4) Kandouz, M. *Cancer Metastasis Rev.* **2012**, *31*, 353.
(5) Xi, H.-Q.; Wu, X.-S.; Wei, B.; Chen, L. *Journal of Cellular and Molecular Medicine* **2012**, *16*, 2894.
(6) Pasquale, E. B. *Nat. Rev. Cancer* **2010**, *10*, 165.
(7) Boyd, A. W.; Bartlett, P. F.; Lackmann, M. *Nat. Rev. Drug Discovery* **2014**, *13*, 39.
(8) Faruqi, M. *Nat. Rev. Drug Discovery* **2012**, *11*, 747.
(9) Chiu, S.-T.; Chang, K.-J.; Ting, C.-H.; Shen, H.-C.; Li, H.; Hsieh, F.-J. *Carcinogenesis* **2009**, *30*, 1475.
(10) Ji, X.-D.; Li, G.; Feng, Y.-X.; Zhao, J.-S.; Li, J.-J.; Sun, Z.-J.; Shi, S.; Deng, Y.-Z.; Xu, J.-F.; Zhu, Y.-Q.; Koeffler, H. P.; Tong, X.-J.; Xie, D. *Cancer Res.* **2011**, *71*, 1156.

DOI: 10.1021/jacs.6b05483
J. Am. Chem. Soc. 2016, 138, 10554−10560

(11) Li, G.; Ji, X.-D.; Gao, H.; Zhao, J.-S.; Xu, J.-F.; Sun, Z.-J.; Deng, Y.-Z.; Shi, S.; Feng, Y.-X.; Zhu, Y.-Q.; Wang, T.; Li, J.-J.; Xie, D. *Nat. Commun.* **2012**, *3*, 667.
(12) Jägle, S.; Rönsch, K.; Timme, S.; Andrlová, H.; Bertrand, M.; Jäger, M.; Proske, A.; Schrempp, M.; Yousaf, A.; Michoel, T.; Zeiser, R.; Werner, M.; Lassmann, S.; Hecht, A. *Proc. Natl. Acad. Sci. U. S. A.* **2014**, *111*, 4886.
(13) Binns, K. L.; Taylor, P. P.; Sicheri, F.; Pawson, T.; Holland, S. J. *Mol. Cell. Biol.* **2000**, *20*, 4791.
(14) Downward, J.; Parker, P.; Waterfield, M. D. *Nature* **1984**, *311*, 483.
(15) Walton, G. M.; Chen, W. S.; Rosenfeld, M. G.; Gill, G. N. *J. Biol. Chem.* **1990**, *265*, 1750.
(16) Ballotti, R.; Lammers, R.; Scimeca, J. C.; Dull, T.; Schlessinger, J.; Ullrich, A.; Van Obberghen, E. *EMBO J.* **1989**, *8*, 3303.
(17) Islam, K. *ACS Chem. Biol.* **2015**, *10*, 343.
(18) Lampson, M. A.; Kapoor, T. M. *Cell* **2006**, *126*, 827.
(19) Qiao, L.; Choi, S.; Case, A.; Gainer, T. G.; Seyb, K.; Glicksman, M. A.; Lo, D. C.; Stein, R. L.; Cuny, G. D. *Bioorg. Med. Chem. Lett.* **2009**, *19*, 6122.
(20) Cohen, M. S.; Zhang, C.; Shokat, K. M.; Taunton, J. *Science* **2005**, *308*, 1318.
(21) Knight, Z. A.; Shokat, K. M. *Cell* **2007**, *128*, 425.
(22) Cohen, M. S.; Hadjivassiliou, H.; Taunton, J. *Nat. Chem. Biol.* **2007**, *3*, 156.
(23) Henise, J. C.; Taunton, J. *J. Med. Chem.* **2011**, *54*, 4133.
(24) Blair, J. A.; Rauh, D.; Kung, C.; Yun, C.-H.; Fan, Q.-W.; Rode, H.; Zhang, C.; Eck, M. J.; Weiss, W. A.; Shokat, K. M. *Nat. Chem. Biol.* **2007**, *3*, 229.
(25) Zhou, W.; Ercan, D.; Chen, L.; Yun, C.-H.; Li, D.; Capelletti, M.; Cortot, A. B.; Chirieac, L.; Iacob, R. E.; Padera, R.; Engen, J. R.; Wong, K.-K.; Eck, M. J.; Gray, N. S.; Janne, P. A. *Nature* **2009**, *462*, 1070.
(26) Zhang, T.; Inesta-Vaquera, F.; Niepel, M.; Zhang, J.; Ficarro, S. B.; Machleidt, T.; Xie, T.; Marto, J. A.; Kim, N.; Sim, T.; Laughlin, J. D.; Park, H.; LoGrasso, P. V.; Patricelli, M.; Nomanbhoy, T. K.; Sorger, P. K.; Alessi, D. R.; Gray, N. S. *Chem. Biol.* **2012**, *19*, 140.
(27) Kwiatkowski, N.; Zhang, T.; Rahl, P. B.; Abraham, B. J.; Reddy, J.; Ficarro, S. B.; Dastur, A.; Amzallag, A.; Ramaswamy, S.; Tesar, B.; Jenkins, C. E.; Hannett, N. M.; McMillin, D.; Sanda, T.; Sim, T.; Kim, N. D.; Look, T.; Mitsiades, C. S.; Weng, A. P.; Brown, J. R.; Benes, C. H.; Marto, J. A.; Young, R. A.; Gray, N. S. *Nature* **2014**, *511*, 616.
(28) Overman, R. C.; Debreczeni, J. E.; Truman, C. M.; McAlister, M. S.; Attwood, T. K. *Protein Sci.* **2014**, *23*, 627.
(29) Scheffler, M.; Di Gion, P.; Doroshyenko, O.; Wolf, J.; Fuhr, U. *Clin. Pharmacokinet.* **2011**, *50*, 371.
(30) Witt, J. J.; Roskoski, R., Jr *Anal. Biochem.* **1975**, *66*, 253.
(31) Bardelle, C.; Barlaam, B.; Brooks, N.; Coleman, T.; Cross, D.; Ducray, R.; Green, I.; Brempt, C. L.-v. d.; Olivier, A.; Read, J. *Bioorg. Med. Chem. Lett.* **2010**, *20*, 6242.
(32) Weerapana, E.; Wang, C.; Simon, G. M.; Richter, F.; Khare, S.; Dillon, M. B. D.; Bachovchin, D. A.; Mowen, K.; Baker, D.; Cravatt, B. F. *Nature* **2010**, *468*, 790.
(33) Lanning, B. R.; Whitby, L. R.; Dix, M. M.; Douhan, J.; Gilbert, A. M.; Hett, E. C.; Johnson, T. O.; Joslyn, C.; Kath, J. C.; Niessen, S.; Roberts, L. R.; Schnute, M. E.; Wang, C.; Hulce, J. J.; Wei, B.; Whiteley, L. O.; Hayward, M. M.; Cravatt, B. F. *Nat. Chem. Biol.* **2014**, *10*, 760.
(34) Birgbauer, E.; Cowan, C. A.; Sretavan, D. W.; Henkemeyer, M. *Development* **2000**, *127*, 1231.
(35) Holder, N.; Klein, R. *Development* **1999**, *126*, 2033.
(36) Liu, Y.; Gray, N. S. *Nat. Chem. Biol.* **2006**, *2*, 358.
(37) Pargellis, C.; Tong, L.; Churchill, L.; Cirillo, P. F.; Gilmore, T.; Graham, A. G.; Grob, P. M.; Hickey, E. R.; Moss, N.; Pav, S.; Regan, J. *Nat. Struct. Biol.* **2002**, *9*, 268.
(38) Chun, E.; Thompson, A. A.; Liu, W.; Roth, C. B.; Griffith, M. T.; Katritch, V.; Kunken, J.; Xu, F.; Cherezov, V.; Hanson, M. A.; Stevens, R. C. *Structure* **2012**, *20*, 967.

DOI: 10.1021/jacs.6b05483
J. Am. Chem. Soc. 2016, 138, 10554−10560